ChemComm

COMMUNICATION

View Article Online
View Journal | View Issue

Cite this: *Chem. Commun.*, 2025, **61**, 5190

Received 9th November 2024,
Accepted 3rd March 2025

DOI: 10.1039/d4cc05979d

rsc.li/chemcomm

BODIPY-coelenterazine conjugates as self-illuminating substrates for NanoLuc†

Valeska Viereckt,[a] Frank Abendroth,[a] Alexander Schauerte,[b] Marina Gerhard,[b] Crispin Lichtenberg,[a] Dmitri Kosenkov[cd] and Olalla Vázquez*[ae]

We report how the conjugation of coelenterazine (CTZ) to BODIPY retains its activity as a versatile substrate for luciferase-type enzymes opening the possibility of taking advantage of BODIPY's fluorescent properties and capacity to generate singlet oxygen. Bioluminescence imaging-guided photodynamic therapy or $^1O_2$-triggered drug release are potential applications of these conjugates.

Bioluminescence—light emission by living organisms—is a powerful tool for studying biological processes because it relies on enzymes, enabling high sensitivity and biocompatibility.[1] Consequently, bioluminescent systems are widely used in detection.[2,3] Beyond cell tracking and reporter assays, the current bioluminescence toolkit has led to pioneering probes capable of monitoring metabolites at the point of care,[4] radiometric sensors,[5,6] uncaging inducers,[7] signal-transduction triggers[8] and photosensitiser activators.[9] In many of them, the light generated from luciferase-type substrates drives bioluminescence resonance energy transfer (BRET), facilitating longer-wavelength emissions and internal activation by self-illumination. BRET reduces heat conversion and photobleaching and allows prolonged homogenous measurements,[10,11] minimising the challenges associated with external excitation. Recent BRET systems involved engineered small luciferases linked to fluorescent or phototoxic proteins,[12] like KillerRed[13] and miniSOG,[14] for either tunable emissions[15] or singlet oxygen ($^1O_2$) production in cancer therapy.[16] While genetically encoded tools are valuable, dye-substrate conjugates can enhance BRET by reducing the donor-to-acceptor distance. Besides, their smaller size should also minimise physiological interference and offer a simpler implementation. Along these lines, significant efforts have been devoted to synthesising derivatives of the luciferase-type substrate coelenterazine (CTZ).[17] Unlike conventional D-luciferin, CTZ does not require ATP for activation. To improve optical performance, modifications of CTZ[18–21] and dye conjugates[19] were reported. Surprisingly, to our knowledge, BODIPY-CTZ conjugates remain unexplored despite their spectral overlap (Fig. 1) and the excellent spectroscopic properties of these fluorophores. Of note, BODIPY can easily turn into effective photosensitisers by halogenation,[22] which gives versatility to these potential BRET probes. Herein, we designed novel substrates for the semisynthetic enzyme NanoLuc (NLuc).[23] NLuc outperforms traditional luciferase enzymes in brightness, stability and size. In 2015, NLuc's potential was further expanded by the development of its split version, NanoBiT.[24] NanoBiT consists of an optimised 18 kDa fragment LgBiT and high-affinity peptide HiBiT (K_d = 700 pM). Since BRET efficiency depends on donor–acceptor proximity and dipole orientation, we envisioned conjugates with different linker lengths (**3** & **5**) and the halogenated analogues (**4** & **6**).

Two synthetic routes were explored for the CTZ core (Scheme 1). For conjugates with the expected longer linker (**5** & **6**), CTZ **9** was obtained by a Horner–Wadsworth–Emmons olefination.[25] Subsequent acetylation with excess of acetic anhydride increased the precursor's stability. For the shorter-linker conjugates (**3** & **4**), the synthesis hinged on a palladium-catalyzed Hartwig–Buchwald *N*-arylation of chloropyrazine **10** with α-amino ester **11** yielding the key intermediate *N*-arylester **12**.[26] This was then converted into the *O*-acetylated CTZ **14** *via* an *in situ*-generated acid salt. The latter procedure (Scheme 1B) was more economical and easily scalable. Finally, the *O*-acetylated CTZ **13** and **14** were conjugated to the corresponding BODIPY moieties *via* NHS ester formation. Conveniently, the coupling reaction also led to hydrolysis of the *O*-acetyl group. The resulting conjugates **3–6** were stored under N_2 atmosphere in the dark at −80 °C to avoid CTZ decomposition.

[a] *Department of Chemistry, Marburg University, Marburg, Germany. E-mail: olalla.vazquez@staff.uni-marburg.de*
[b] *Department of Physics and Materials Science Center, Marburg University, Marburg, Germany*
[c] *Princeton Precision Health (PPH), Princeton University, Princeton, USA*
[d] *Lewis-Sigler Institute for Integrative Genomics, Princeton University, Princeton, USA*
[e] *Centre for Synthetic Microbiology (SYNMIKRO), University of Marburg, Marburg, Germany*

† Electronic supplementary information (ESI) available. See DOI: https://doi.org/10.1039/d4cc05979d

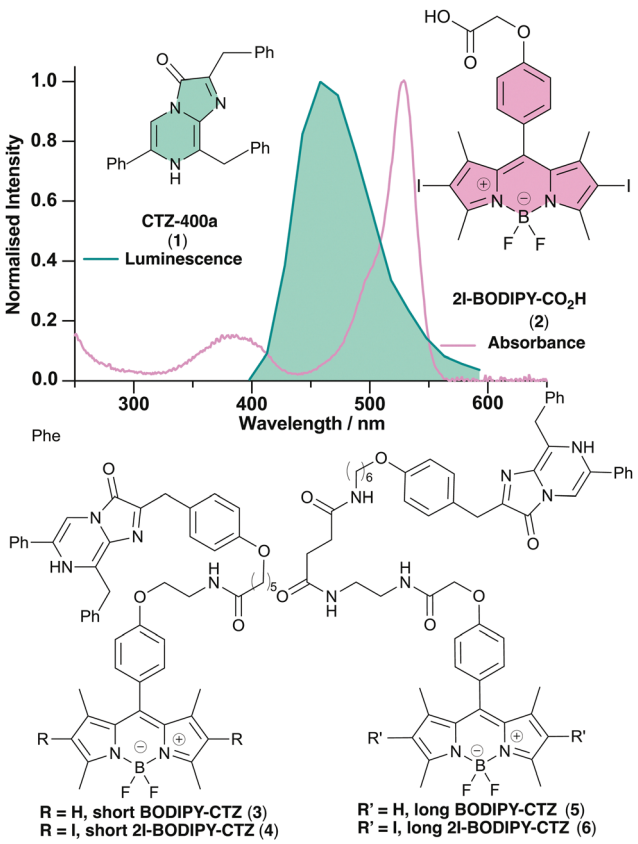

Fig. 1 Top: Evidence of BRET by luminescence and absorbance spectral overlap. Down: Chemical structure of the aim BODIPY-CTZ probes as NLuc substrates.

Once synthesized, we investigated the ability of the conjugates to generate $^1O_2$ under irradiation using 1,3-diphenylisobenzofuran (DPBF) as a trap[27] and compared the results to the unconjugated photosensitizer **2** (Table SR1, SR2 and Fig. SR1, SR2, ESI†). As expected, both conjugates displayed comparable photosensitizing capacity. Interestingly, **2**, which lacks CTZ, surpassed them by ~33%. To confirm that this difference was not due to a decrease in available $^1O_2$ by reacting with the susceptible CTZ core, we added up to 277 eq of CTZ-400a (**1**) to **2** (Fig. SR3, ESI†). Although **1** slightly decreased the rate of DPBF consumption, the conjugates **4** and **6** still displayed the slowest kinetics. Of note, CTZ hardly absorbed at 517 nm (Fig. SR4 and SR5, ESI†). Next, we examined whether the conjugation impacted the fluorescence of the non-halogenated analogues **3** and **5** (Fig. SR6, SR7 and Table SR3, ESI†). As before, fluorescence was lower for the conjugates **3** (Φ_F = 0.243) and **5** (Φ_F = 0.269) than for BODIPY without CTZ **22** (Φ_F = 0.604).

To investigate these photochemical behaviours, we conducted excitation energy transfer modelling based on Förster resonance energy transfer (FRET) theory,[28] as implemented in the PyFREC software[29] and *ab initio* molecular models. In our FRET modelling (Tables SR4 and SR5, ESI†), we assumed that the excitation energy of 2I-BODIPY is transferred *via* a FRET mechanism from the 2I-BODIPY donor to the CTZ acceptor. This FRET interaction facilitates photoexcitation energy transfer, which ultimately reduces the energy available for $^1O_2$ production or fluorescence emission. This is also evident from the experimentally measured fluorescence lifetimes, where the lifetime of BODIPY-CO_2H (4.581 ± 0.030 ns) slightly decreases upon the addition of CTZ, dropping to 4.367 ± 0.032 ns for 1 : 10 BODIPY-CO_2H-to-CTZ concentrations. Additionally, short and long conjugates **3** and **5**, which feature covalently bound CTZ groups, exhibit even shorter lifetimes 3.617 ± 0.048 ns and 3.819 ± 0.041 ns, respectively. The decreased energy available for these processes is a direct result of the efficient FRET mechanism. Furthermore, although conjugate **6** (and **5**) has a donor–acceptor distance longer by approximately 30% compared to shorter conjugates, the mutual orientation factor of the donor and acceptor groups is ~4–6 times more favourable in the longer conjugates **6** (and **5**) (Table SR5 and Fig. 2, ESI†). This orientation factor contributes to faster computed FRET rates in these shorter conjugates (Table SR5, ESI†), which is likely an overestimation because modelling is based on one static minimal energy molecular geometry while an ensemble of molecular geometries exists in solution. Despite that experimentally, both short and long conjugates exhibit similar quantum yields, suggesting that the longer distance in conjugate **6** is offset by less favourable orientation factors in conjugate **4**, likely due to the higher rigidity of the shorter linker. Finally, lower fluorescence lifetimes and higher FRET efficiencies were found for **3** and **5** (Table S1, Fig. S1–S6, Table SR3 and Fig. SR7, ESI†).

While direct BRET modelling is beyond this work's scope, we applied FRET theory to explore possible mechanisms of energy transfer for the BRET model. Although our FRET model does not yield absolute BRET rates, its distance- and orientation-dependent factors are analogous to those of BRET. Our modelling suggests that if the BRET excitation donor is (an oxidized form of) CTZ with the BODIPY moiety acting as the acceptor, then, again, a longer conjugate should result in more optimal donor–acceptor alignment and a faster BRET rate compared to the shorter conjugate (Table SR5, ESI†).

Next, we explored if NanoBiT could oxidize the conjugates to generate light. We first verified LgBiT-HiBiT enzymatic activity using CTZ-400a (**1**) (Fig. SR8, ESI†).[26] Gratifyingly, both non-halogenated conjugates (**3** and **5**) produced detectable light but less than **1** (Fig. 3A). Consistent with our calculations, the long conjugate **5** exhibited a faster BRET rate and higher bioluminescence than the shorter one **3**, possibly due to the more rigid, shorter linker chain in conjugate **3** and/or its molecular interactions. As previously reported for the conversion of CTZ derivatives by NLuc,[26] the kinetics of **5** were best described by the substrate-inhibition model (Fig. SR9, ESI†), displaying the highest signal with a characteristic flash-type bioluminescence. In contrast, the standard Michaelis–Menten model provided the best fit for **3**. To evaluate whether the observed bioluminescence can activate the attached BODIPY *via* BRET, we recorded luminescence in the presence of LgBiT and HiBiT (Fig. 3B). BRET was detected for **5** (λ_{max} = 518 nm) but not for **3** (λ_{max} = 458 nm), which aligns with our kinetics studies.

Encouraged by the BRET efficiency of **5** and the ability of the conjugates **4** and **6** to produce $^1O_2$ under irradiation (Table 1),

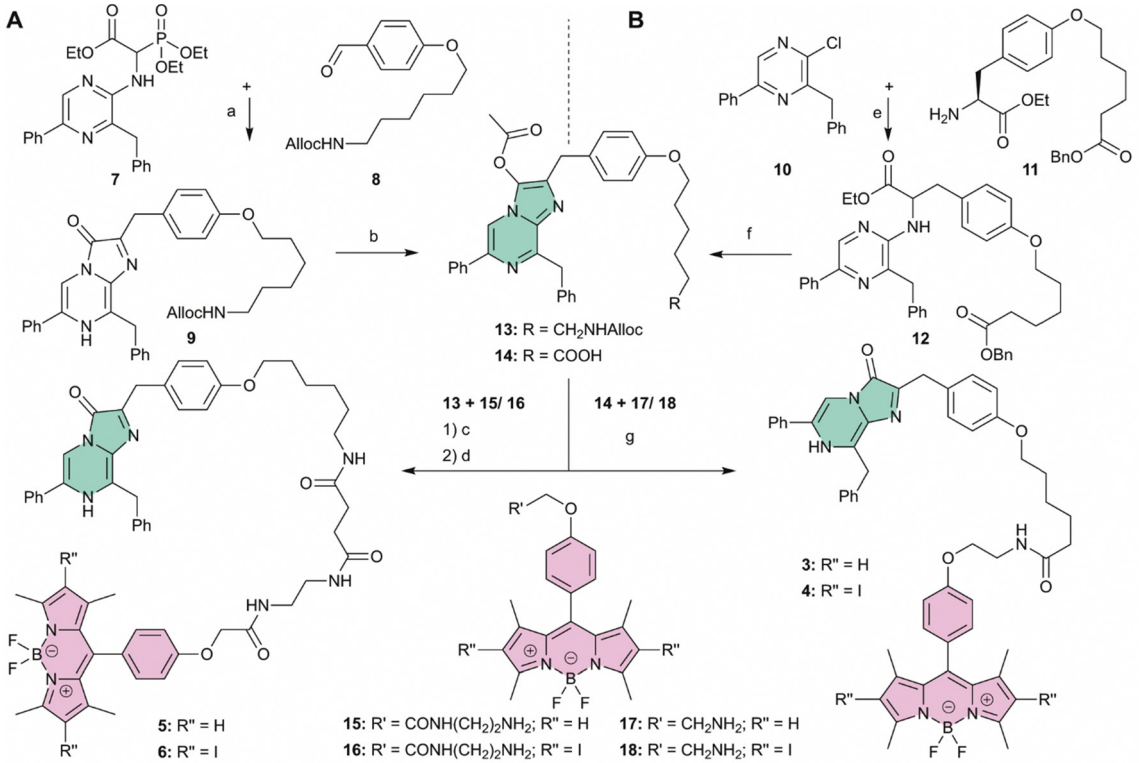

Scheme 1 (A) Synthesis of long BODIPY- (**5**) and 2I-BODIPY-CTZ (**6**) conjugates: (a) (1) TMG, MeOH, rt, 2 h; (2) $NaBH_4$, DCM/MeOH 1 : 1, rt, 1 h; 27%; (b) Ac_2O, rt, 2 h; 99%; (c) succinic anhydride, $Pd(PPh_3)_4$, $PhSiH_3$, DMF, rt, 45 min; 83%; (d) (1) NHS, DIC, THF, rt, 45 min; (2) **15**/**16**, NMM, THF, rt, 1 h; 25% for **5**; 27% for **6**. (B) Synthesis of short BODIPY- (**3**) and 2I-BODIPY-CTZ (**4**) conjugates: (e) Cs_2CO_3, $Pd(OAc)_2$, BINAP, MeCN, 60 °C, 12 h; 76%; (f) (1) NaOH, THF, rt, 16 h; (2) Ac_2O, THF, rt, 2 h; 38%; (g) for **3**: (1) NHS, DIC, THF, rt, 2.5 h; (2) **17**, NMM, THF, rt, 2.5 h; 37%; for **4**: (1) NHS, DIC, THF, rt, 2.5 h; (2) **18**, NMM, DMF, rt, 1.5 h; 42%.

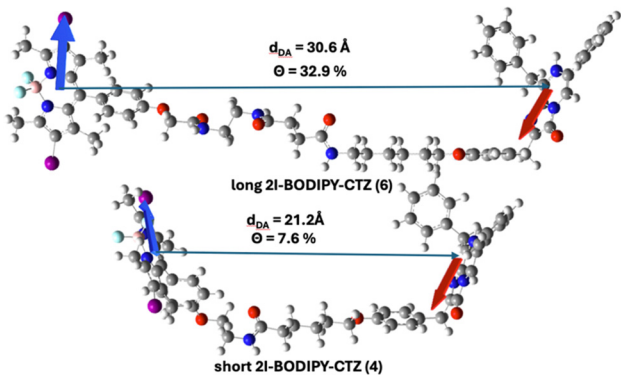

Fig. 2 Although the short 2I-BODIPY-CTZ (**4**) conjugate has a shorter donor–acceptor distance (d_{DA}) than the long 2I-BODIPY-CTZ (**6**), the mutual orientation factor (Θ) of the transition dipole moments (red and blue arrows) is less favourable for FRET. This trend also holds for **3** and **5** (see Table SR5, ESI†).

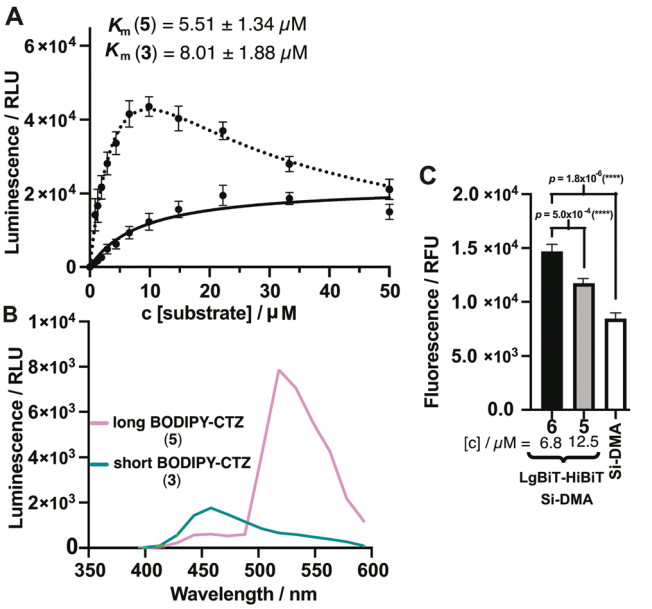

Fig. 3 (A) K_m of **3** and **5** using LgBiT-HiBiT. Mean value of three independent measurements after 5 min of substrate addition. (B) Luminescence spectra of **3** and **5** at 14.8 μM in 50 mM Tris pH = 7.5, 150 mM NaCl, 0.005% Igepal CA-630 and 0.1 g L^{-1} BSA. (C) $^1O_2$ detection using 25 μM Si-DMA, 12.5 μM of **5** or 6.8 μM of **6** in 10 mM phosphate buffer (pH 7.4), 100 mM NaCl, 20% glycerol. ****$p < 0.0001$.

we investigated if their bioluminescence could yield detectable $^1O_2$. Several challenges arose: (i) reduced Φ_Δ due to CTZ conjugation; (ii) solubility limitations (up to 50 μM); (iii) CTZ instability in solubilizing organic solvents; (iv) inherent difficulty in $^1O_2$ detection. Initially, we tested NLuc-expressing cells with our conjugates. Unfortunately, the toxicity was modest

Table 1 $^1O_2$ quantum yields (Φ_Δ) in MeOH relative to erythrosine B (Φ_Δ = 0.62)[30] using a LED source (λ_{em} = 517 nm)

Compound	I_a 517 nm, 5.4 μM	k^a [s^{-1} 10^{-3}]	$\Phi_\Delta{}^b$
2I-BODIPY-CO_2H (**2**)	0.476 ± 0.020	32.6 ± 1.48	0.719
Short 2I-BODIPY-CTZ (**4**)	0.418 ± 0.022	19.4 ± 0.32	0.490
Long 2I-BODIPY-CTZ (**6**)	0.399 ± 0.020	18.1 ± 2.36	0.476

[a] k reaction constant of $^1O_2$ generation *via* DPBF decomposition. [b] Mean value of three independent measurements with errors ≤± 9%. I_a = absorbance.

without differences between halogenated and non-halogenated conjugates (Fig. SR10 and SR11, ESI†). Singlet oxygen sensor green (SOSG) and electron paramagnetic resonance (EPR) analysis with 4-OH-TEMP were unsuitable due to the intrinsic requirements of our system, *i.e.*, emission-spectrum overlap, photosensitizer concentrations >1 μM and physiological conditions (pH < 8). However, the far-red probe Si-DMA[31] displayed a statistically significant response with **6**, using almost half of **5** concentration (Fig. 3C and Fig. SR12, ESI†). Interestingly, the enzyme alone appeared to interact with Si-DMA, increasing its fluorescence (Fig. SR13 ESI,† K_d = 17.5 ± 5.0 μM) but not with bovine serum albumin (BSA).

We thank Prof. Tallarek and Dr Thomas Roider (photometry); Prof. Koert (infrared spectroscopy); Prof. Hideg and Dr Carmielli (EPR); Marburg University for financial support.

Data availability

The supporting data are provided in the ESI.†

Conflicts of interest

There are no conflicts to declare.

References

1 P. J. Herring, *Nature*, 1977, **267**, 788–793.
2 S. Liu, Y. Su, M. Z. Lin and J. A. Ronald, *ACS Chem. Biol.*, 2021, **16**, 2707–2718.
3 A. C. Love and J. A. Prescher, *Cell Chem. Biol.*, 2020, **27**, 904–920.
4 Q. Yu, L. Xue, J. Hiblot, R. Griss, S. Fabritz, C. Roux, P. A. Binz, D. Haas, J. G. Okun and K. Johnsson, *Science*, 2018, **361**, 1122–1126.
5 L. A. Stoddart, E. K. M. Johnstone, A. J. Wheal, J. Goulding, M. B. Robers, T. Machleidt, K. V. Wood, S. J. Hill and K. D. G. Pfleger, *Nat. Methods*, 2015, **12**, 661–663.
6 M. Soave, R. Heukers, B. Kellam, J. Woolard, M. J. Smit, S. J. Briddon and S. J. Hill, *Cell Chem. Biol.*, 2020, **27**, 1250–1261 e1255.
7 D. Chang, E. Lindberg, S. Feng, S. Angerani, H. Riezman and N. Winssinger, *Angew. Chem., Int. Ed.*, 2019, **58**, 16033–16037.
8 J. R. Zenchak, B. Palmateer, N. Dorka, T. M. Brown, L. M. Wagner, W. E. Medendorp, E. D. Petersen, M. Prakash and U. Hochgeschwender, *J. Neurosci. Res.*, 2020, **98**, 458–468.
9 Y. R. Kim, S. Kim, J. W. Choi, S. Y. Choi, S. H. Lee, H. Kim, S. K. Hahn, G. Y. Koh and S. H. Yun, *Theranostics*, 2015, **5**, 805–817.
10 N. Boute, R. Jockers and T. Issad, *Trends Pharmacol. Sci.*, 2002, **23**, 351–354.
11 G. Choy, S. O'Connor, F. E. Diehn, N. Costouros, H. R. Alexander, P. Choyke and S. K. Libutti, *Biotechniques*, 2003, **35**, 1022–1030.
12 E. H. Kim, S. Park, Y. K. Kim, M. Moon, J. Park, K. J. Lee, S. Lee and Y. P. Kim, *Sci. Adv.*, 2020, **6**, eaba3009.
13 M. E. Bulina, D. M. Chudakov, O. V. Britanova, Y. G. Yanushevich, D. B. Staroverov, T. V. Chepurnykh, E. M. Merzlyak, M. A. Shkrob, S. Lukyanov and K. A. Lukyanov, *Nat. Biotechnol.*, 2006, **24**, 95–99.
14 X. Shu, V. Lev-Ram, T. J. Deerinck, Y. Qi, E. B. Ramko, M. W. Davidson, Y. Jin, M. H. Ellisman and R. Y. Tsien, *PLoS Biol.*, 2011, **9**, e1001041.
15 J. Hiblot, Q. Yu, M. D. B. Sabbadini, L. Reymond, L. Xue, A. Schena, O. Sallin, N. Hill, R. Griss and K. Johnsson, *Angew. Chem., Int. Ed.*, 2017, **56**, 14556–14560.
16 E. I. Shramova, S. P. Chumakov, V. O. Shipunova, A. V. Ryabova, G. B. Telegin, A. V. Kabashin, S. M. Deyev and G. M. Proshkina, *Light: Sci. Appl.*, 2022, **11**, 38.
17 W. W. Lorenz, M. J. Cormier, D. J. O'Kane, D. Hua, A. A. Escher and A. A. Szalay, *J. Biolumin. Chemilumin.*, 1996, **11**, 31–37.
18 T. Jiang, X. Yang, Y. Zhou, I. Yampolsky, L. Du and M. Li, *Org. Biomol. Chem.*, 2017, **15**, 7008–7018.
19 R. Nishihara, E. Hoshino, Y. Kakudate, S. Kishigami, N. Iwasawa, S. I. Sasaki, T. Nakajima, M. Sato, S. Nishiyama, D. Citterio, K. Suzuki and S. B. Kim, *Bioconjugate Chem.*, 2018, **29**, 1922–1931.
20 P. Nadal Rodriguez, O. Ghashghaei, A. M. Schoepf, S. Benson, M. Vendrell and R. Lavilla, *Angew. Chem., Int. Ed.*, 2023, **135**, e202303889.
21 G. Kamiya, N. Kitada, T. Furuta, S. Thangudu, A. Natarajan, R. Paulmurugan, S. B. Kim and S. A. Maki, *Bioconjugate Chem.*, 2024, **35**, 1391–1401.
22 A. Gorman, J. Killoran, C. O'Shea, T. Kenna, W. M. Gallagher and D. F. O'Shea, *J. Am. Chem. Soc.*, 2004, **126**, 10619–10631.
23 M. P. Hall, J. Unch, B. F. Binkowski, M. P. Valley, B. L. Butler, M. G. Wood, P. Otto, K. Zimmerman, G. Vidugiris, T. Machleidt, M. B. Robers, H. A. Benink, C. T. Eggers, M. R. Slater, P. L. Meisenheimer, D. H. Klaubert, F. Fan, L. P. Encell and K. V. Wood, *ACS Chem. Biol.*, 2012, **7**, 1848–1857.
24 A. S. Dixon, M. K. Schwinn, M. P. Hall, K. Zimmerman, P. Otto, T. H. Lubben, B. L. Butler, B. F. Binkowski, T. Machleidt, T. A. Kirkland, M. G. Wood, C. T. Eggers, L. P. Encell and K. V. Wood, *ACS Chem. Biol.*, 2016, **11**, 400–408.
25 A. Shakhmin, M. P. Hall, T. Machleidt, J. R. Walker, K. V. Wood and T. A. Kirkland, *Org. Biomol. Chem.*, 2017, **15**, 8559–8567.
26 E. P. Coutant, S. Goyard, V. Hervin, G. Gagnot, R. Baatallah, Y. Jacob, T. Rose and Y. L. Janin, *Org. Biomol. Chem.*, 2019, **17**, 3709–3713.
27 G. Linden, L. Zhang, F. Pieck, U. Linne, D. Kosenkov, R. Tonner and O. Vazquez, *Angew. Chem., Int. Ed.*, 2019, **58**, 12868–12873.
28 T. Főrster, *Discuss. Faraday Soc.*, 1959, **27**, 7–17.
29 D. Kosenkov, *J. Comput. Chem.*, 2022, **43**, 1320–1328.
30 J. J. M. Lamberts, D. R. Schumacher and D. C. Neckers, *J. Am. Chem. Soc.*, 1984, **106**, 5879–5883.
31 S. Kim, T. Tachikawa, M. Fujitsuka and T. Majima, *J. Am. Chem. Soc.*, 2014, **136**, 11707–11715.